Langmuir

Letter

pubs.acs.org/Langmuir

Tuning Kinetics to Control Droplet Shapes on Chemically Striped Patterned Surfaces

H. Patrick Jansen,[†] Kai Sotthewes,[†] Christian Ganser,[‡,§] Christian Teichert,[‡] Harold J. W. Zandvliet,[†] and E. Stefan Kooij*,[†]

[†]Physics of Interfaces and Nanomaterials, MESA+ Institute for Nanotechnology, University of Twente, P.O. Box 217, 7500 AE Enschede, The Netherlands

[‡]Institute of Physics, Montanuniversitaet Leoben, Franz-Josef-Strasse 18, A-8700, Leoben, Austria

[§]CD-Laboratory for Surface Chemical and Physical Fundamentals of Paper Strength, Graz University of Technology, 8010 Graz, Austria

ABSTRACT: The typically elongated shape of droplets on chemically microstriped surfaces has been suggested to depend strongly on the kinetics during deposition. Here, we unequivocally establish the importance of impact kinetics by comparing the geometry of pico- to microliter droplets deposited from an inkjet nozzle with those obtained by conventional deposition from a syringe. For large Weber numbers, the strongly enhanced spreading during the impact in combination with direction-dependent pinning of the contact line gives rise to more spherical droplets with a low aspect ratio. The impact energy can be minimized by the prolonged firing of small picoliter droplets to form larger droplets or, as shown in the past, by using high-viscosity liquids. In the first case, the impact energy is absorbed by the liquid already present, therewith reducing the impact diameter and consequently forming markedly more elongated droplets.

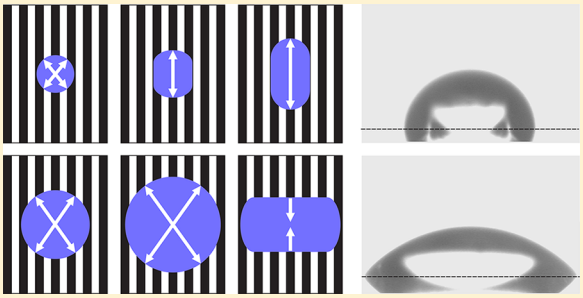

INTRODUCTION

Controlling surface wettability is attracting a significant amount of scientific attention in many research areas, including fluid physics, materials science, and interface physics. Numerous theoretical,[1−6] computational,[7−11] and experimental[12−17] studies have been conducted on chemically heterogeneous and topographically structured surfaces. By controlling the surface wettabillity, droplets can be moved over a surface using a gradient in surface energy.[18,19] A recent review covers the latest advances in this field.[20]

Droplet impact dynamics on surfaces with anisotropic wettability has been studied by Kannan and Sivakumar.[21,22] Léopoldès and Bucknall[23] identified spreading regimes as a function of the wettability contrast on a microstriped surface; a high wettability contrast between the stripes leads to elongated droplets. Bliznyuk et al.[15] investigated the effect of varying stripe widths on the final droplet shape for high wettability contrast. The volumes typically used for these studies are in the microliter range, where the droplet covers many stripes. In this letter, our focus is on the behavior of considerably smaller droplets, which still cover multiple stripes on chemically microstriped surfaces. On the basis of the results, we will convincingly demonstrate the importance of kinetics in the final droplet shape. We compare our results to experiments and simulations by Kusumaatmaja et al.,[24] who studied the shape of droplets on corrugated surfaces showing that the deposition method, and therewith the path the droplet follows, is important to the final shape.

EXPERIMENTAL DETAILS

Our substrates, consisting of alternating hydrophobic and hydrophilic stripes with anisotropic wetting properties (Figure 1a), are created using self-assembled perfluordecyltrichlorosilane (PFDTS, ABCR Germany) monolayers on oxide-coated silicon wafers; details are given elsewhere.[15] The global surface energy is a function of the relative widths of the PFDTS stripes with respect to those of the oxide stripes. This can be expressed by the parameter $\alpha = w_{PFDTS}/w_{SiO_2}$, where w denotes the corresponding stripe width. A surface pattern with a low (high) α has broader hydrophilic (hydrophobic) stripes in comparison to other stripes, resulting in a relatively hydrophilic (hydrophobic) surface. Typical stripe widths are between 2 and 36 μm; α values in the range of 0.125−5 were realized using different absolute stripe widths. For α values in the range of 0.25 until 2, at least three different absolute widths for both stripes are used, leading to different periodicities of the pattern.

Microliter droplets are created by employing a computer-controlled syringe (OCA15+ goniometer, Dataphysics, Germany); the droplet volume, typically in the microliter range, is accurate to within 5%. Two cameras are used (parallel and perpendicular to the stripes) to characterize the droplet shape in terms of the dimensions and contact angles; the latter are accurate to within 0.5°. The aspect ratio AR is defined as the quotient of droplet sizes L and W along and perpendicular to the stripes, respectively.

Picoliter droplets are created using a picoliter goniometer (Kruss DSA 100M) equipped with a piezo-driven inkjet print head capable of

Received: June 24, 2012
Revised: September 5, 2012
Published: September 6, 2012

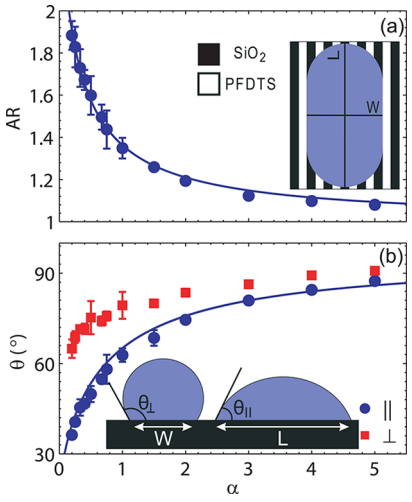

Figure 1. (a) Aspect ratio AR (see the text) of 1 μL water droplets as a function of α, gently deposited using a syringe. The solid line is a guide to the eye. The inset depicts a schematic overview of the droplet on the surface. (b) Contact angles parallel $\theta_{||}$ (blue circles) and perpendicular $\theta_{\perp}$ (red squares) to the stripes as a function of α; the inset depicts the two contact angles. The solid line represent the Cassie–Baxter model (eq 1) with $\theta_{PFDTS} = 96°$ and $\theta_{SiO_2} = 19°$.

producing droplets as small as 50 pL with an accuracy of approximately 10%. The size of the droplets depends on several parameters, such as the piezo voltage, the period of the voltage pulse, and the number of pulses. The velocity of droplets fired from the nozzle amounts to approximately 2–4 m/s, independent of the volume. To enable sufficient time resolution, we also used a modified home-built setup based on the OCA15+ system, in combination with a Photron SA3 camera (up to 10 000 fps).

Home-built software programmed in MatLab is used to analyze the droplets. The edge of the droplet is extracted using a gray-level fit near the border of the droplet. Contact angles are determined by fitting the lower part of the droplet contour (approximately 20–25% of the droplet height) close to the triple line on both sides to a circle. The length of the droplet contour considered in the fitting always exceeds the smallest width of the underlying stripes.

RESULTS AND DISCUSSION

Because of anisotropic spreading on the aforementioned surfaces, a droplet does not exhibit a spherical shape but is typically elongated. Spreading in the direction parallel to the stripes is preferred over spreading perpendicular to them. In the latter case, liquid advancing over subsequent hydrophobic stripes experiences energy barriers, which results in the stick–slip-like motion of the contact line. Because the displacement of the contact line in the parallel direction is not hindered, overall the droplets become elongated.

For the small droplets considered here, produced using an inkjet nozzle, we can use only relatively low viscosity liquids, such as water. To enable comparison with microliter droplets, we plot the aspect ratio in Figure 1a as a function of α for a 1 μL water droplet, corresponding to an initial diameter of D_0 = 1.24 mm. The results for a specific α are averaged for different absolute stripe widths; the error bars represent the standard deviation between the measurements. For lower α, the error increases as a result of the stronger influence of pinning centers on the droplet shape and a small effect of absolute stripe widths (not considered here). A droplet deposited by the syringe spans about 150 to 350 stripes, depending on the absolute width of the stripes. As a reference, contact angles on clean wafers amount to $\theta_{PFDTS} = 106°$ and $\theta_{SiO_2} = 27°$. The advancing and receding angles on pristine surfaces were also measured, amounting to $\theta_{adv} = 116°$ and $\theta_{rec} = 96°$ for PFDTS and $\theta_{adv} = 30°$ and $\theta_{rec} = 21°$ for SiO_2. For low α values, the aspect ratio is high, corresponding to a strongly elongated droplet, whereas for large α the aspect ratio is close to 1 (i.e., a spherical droplet).

In Figure 1b, the contact angles of a 1 μL droplet parallel and perpendicular to the stripes as a function of α are shown. The parallel contact angle can be adequately described by the Cassie–Baxter model,[25] modified by rewriting it as a function of α:

$$\cos(\theta_{||}) = \frac{\cos(\theta_{SiO_2}) + \alpha \cos(\theta_{PDFTS})}{1 + \alpha} \quad (1)$$

The best fit is obtained with $\theta_{PFDTS} = 96°$ and $\theta_{SiO_2} = 19°$, close to the receding angles measured on the pristine surfaces. The perpendicular contact angle $\theta_{\perp}$ is larger than the parallel one $\theta_{||}$. Because of the pinning of the contact line at the border between PFDTS and SiO_2 stripes, $\theta_{\perp}$ is close to the contact angle on PFDTS. However, for lower values of α this contact angle starts to decrease.

We now turn to markedly smaller droplets, typically in the picoliter range, to investigate the effect of the absolute volume on the anisotropic wetting properties. Droplets with three volumes were used (80 ± 10, 245 ± 19, and 402 ± 54 pL), corresponding to initial droplet diameters of 53, 78, and 92 μm, respectively. In Figure 2, images of the picoliter droplets are

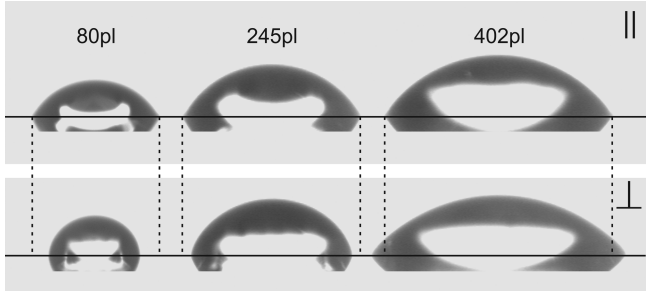

Figure 2. Snapshots of deposited droplets on the surface for different volumes. The α of the surface pattern is 0.5 with PFDTS and SiO_2 stripe widths of 6 and of 12 μm, respectively. The top row shows a side view in the direction parallel to the stripes, and the bottom row shows a side view perpendicular to the stripes. The width of the 80 pL droplet in the perpendicular direction is 65 μm. The solid black line indicates the baseline of the substrate, and the dashed lines indicate the droplet width in the parallel direction.

shown for the two directions and the different volumes. The droplets in the top row show roughly the same contact angle and shape; the width at the baseline increases for higher volumes. The droplets in the bottom row, for the perpendicular direction, do show a different contact angle and shape. The width at the baseline also increases with volume, but the contact angle decreases. For the 80 pL case, the elongation is the largest, as can be seen by the dashed lines. The 245 pL droplet is slightly elongated, and for the 402 pL droplet, the width in the perpendicular direction is larger than in the parallel direction.

In Figure 3a, the AR is plotted as a function of α for the three volumes. Aspect ratio values were obtained from the ratio of separately obtained averaged values for L and W on substrates

dx.doi.org/10.1021/la302551m | Langmuir 2012, 28, 13137–13142

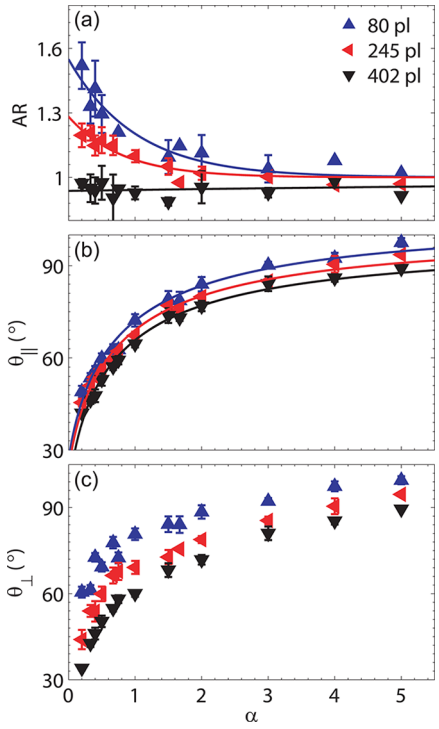

Figure 3. (a) Aspect ratio as a function of α for droplets with different volumes, as deposited by the inkjet nozzle. The solid lines are a guide to the eye. (b, c) Parallel and perpendicular contact angles as a function of α. The solid lines are fits to eq 1 with θ_{PFDTS} = 106, 101, and 98° and θ_{SiO_2} = 27, 23, and 19° for the 80, 245, and 402 pL droplets, respectively.

with different absolute stripe widths; the error bars represent the standard deviation. The aspect ratio of the 80 and 245 pL droplets decreases with increasing α in a manner similar to that for the 1 μL droplets. For the 402 pL droplet, however, the underlying pattern does not seem to affect the shape of the droplet. Apparently, with increasing volume the elongation becomes less pronounced. The maximum aspect ratio is 1.5 for 80 pL and 1.2 for 245 pL and reduces to 1.0 for 402 pL. For comparison, the gently deposited 1 μL droplet has an aspect ratio of 1.9. The number of stripes spanned by the droplets again depends on the absolute stripe width; generally 7−15, 11−25, and 15−33 stripes are covered by the 80, 245, and 402 pL droplets, respectively.

To rationalize the difference between the 1 μL case and the picoliter droplets, we have to consider the contact angles for different volumes. Both $\theta_\perp$ and $\theta_\parallel$ are plotted for the three volumes in Figure 3b,c. Equation 1 is again used to fit the data in Figure 3b. In the figure, a small volume dependence on the parallel contact angle is observed, which is also reflected in the fitting parameters. However, this volume dependence is not sufficient to explain the difference in aspect ratio between the different volumes.

The perpendicular contact angle exhibits a more pronounced dependence on volume. The first fact to notice is that the contact angles decrease for smaller α. This is also the case for the 1 μL droplet, but again absolute values are different. The smallest 80 pL droplet approximates the result in Figure 1 best, but the saturation contact angle is larger. A second observation is that the perpendicular contact angle $\theta_\perp$ is lowest for the largest picoliter droplet. This is in agreement with the fact that $\theta_\perp$ has the largest influence on the aspect ratio whereas the variation of $\theta_\parallel$ with α is almost independent of volume.

To understand the apparent contradiction between the results in Figure 3, (i.e., larger droplets have smaller aspect ratios) and those in Figure 1, which exhibit the largest aspect ratios, we must consider the velocity of the inkjet droplets upon impact at the surface. The impact energy is considerable, and the droplets are "smashed" onto the surface. High-speed movies indeed confirm the considerable deformation of the droplets.

The Weber number, $We = \rho U_0^2 D_0/\sigma$, compares the inertial force to the surface tension, with ρ being the density of the liquid, U_0 being the impact velocity, D_0 being the initial diameter of the droplet, and σ being the surface tension of the liquid. When $We \gg 1$, the inertial force dominates the surface tension, emphasizing the role of impact kinetics. Clanet et al.[26] studied the maximum diameter of a droplet after impact on various surfaces. They concluded that the maximum diameter during the impact event scales as $D_{max}/D_0 \approx We^{1/4}$, independent of the surface wettability.

In Figure 4a, we plot the droplet diameter at the baseline on a homogeneous surface as a function of contact angle for different volumes. The curves are calculated from straightforward geometrics assuming a spherical cap. For small contact

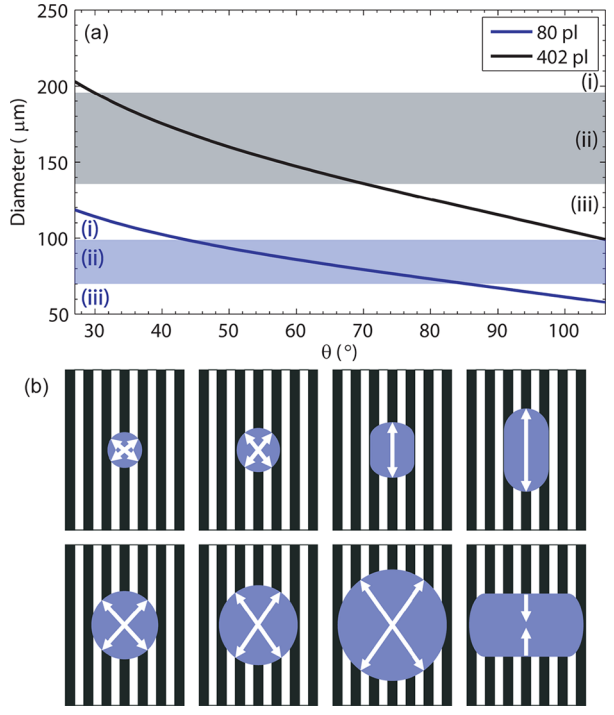

Figure 4. (a) Droplet footprint diameter as a function of contact angle for a homogeneous surface, assuming a spherical cap. The contact angle range corresponds to the α range in our experiments. The shaded areas represent the maximum spreading diameter of actual droplets. The three different regimes (i−iii) discussed in the text are indicated for both volumes. (b) Schematic representation of a droplet spreading on a chemically striped patterned surface depending on the impact diameter of the droplet. The spreading propagation (indicated by white arrows) is shown for two cases: (top row) small droplet spreading similar to microliter droplets in the experiment of Bliznyuk et al.[15] and (bottom row) larger droplet spreading differently because of the much larger kinetic energy of the droplet. To clarify the difference between large (80 pL) and small (402 pL) droplets, the effect is depicted as more pronounced as observed in experiments.

dx.doi.org/10.1021/la302551m | *Langmuir* 2012, 28, 13137−13142

angles, the diameter is larger because the droplet will spread more as compared to the case of large contact angles. For clarity, only two volumes are shown in the graph. Using the scaling law as reported by Clanet et al.,[26] we can also estimate the maximum diameter that a droplet reaches upon hitting the surface. Because the speed is not exactly known, only a diameter range can be estimated, as shown by the shaded horizontal bands. The upper and lower limits correspond to the highest and lowest impact velocities, respectively.

Focusing on a single volume, we can identify three regimes: (i) the diameter of the deposited droplet D_{max} is less than the equilibrium diameter in the global minimum, (ii) the diameter of the deposited droplet D_{max} is similar to the equilibrium diameter, and (iii) the diameter of the deposited droplet D_{max} is greater than the equilibrium value. This leads to different dynamics on the surface. In case i, the fired droplet has not spread beyond the equilibrium diameter and will therefore continue to advance on the surface. In case ii, the diameter of the fired droplet is almost equal to the equilibrium diameter and it can advance or recede, depending on its actual diameter. Because the velocity is not exactly known, this is a mixed regime that can contain both advancing and receding motions of the droplet. In case iii, the diameter of the fired droplet is always larger than the equilibrium diameter, leading to the receding motion of the droplet on the surface.

All three regimes are present for the 80 and 402 pL cases, but not in the same amounts. For the 80 pL case, the droplet will recede when deposited on a surface with a contact angle of 85° or higher. Below a contact angle of 85°, the droplet is either in the mixed regime (ii) or in the advancing regime (i). For the 402 pL case, this is different; a droplet deposited on a surface with a contact angle of 70° or larger has a diameter exceeding the equilibrium value, leading to receding motion. Below a contact angle of 70°, the droplet is in the mixed regime. The advancing regime is almost not present for this volume.

In Figure 4a, the diameter of the deposited droplet is compared to the equilibrium diameter of a droplet on a homogeneous surface with a certain contact angle. In our experiments, we do not have a homogeneous surface but a chemically patterned one. However, we can use the contact angle in the parallel direction, calculated using eq 1, to compare it to our patterns. In Figure 4b, the droplet footprint is schematically shown for a small and a large droplet (top and bottom rows, respectively). When the small droplet impacts, it spreads isotropically with a diameter given in Figure 4a. For small α, this diameter is below the equilibrium diameter, giving rise to further (directional) spreading in regime i or ii along the stripes.

The impact diameter of the largest droplet is so high that it adopts a very flattened shape during impact with a circular footprint. To achieve its equilibrium shape, the droplet retracts to minimize the surface energy. For a surface with $\alpha = 1$, $\theta_{\parallel}$ amounts to 70°, so the 402 pL droplet will always retract. However, receding in the perpendicular direction is strongly hindered because the contact line has to recede over stripes of alternating wettability. Consequently, the width of the droplet will remain constant but its length will decrease, giving rise to an aspect ratio of <1. Indeed, this is what we observe for the 402 pL droplet in Figure 3. For the 245 and 80 pL droplets, this effect is markedly less, leading to elongated droplets along the stripes. The same mechanism is proposed by Kusumaatmaja et al.[24] for corrugated surfaces. In their experiments, they use two deposition techniques: spraying and microcontact printing. In the former case, the droplet adopts an elongated shape in the direction parallel to the grooves because of the advancing motion of the droplet on the surface, which is comparable to what we refer to as regime i. In the latter case, the droplet dewets the surface and retracts, leading to an elongated shape perpendicular to the grooves, comparable to our regime iii. The shape of the droplet is therefore strongly dependent on the regime in which it spreads. The aspect ratio of the 80 pL droplet is still smaller than that of the 1 μL droplet deposited by the syringe, so the impact energy still affects the shape of the smallest droplet. To completely exclude kinetic effects, spreading must always be in regime i, which is clearly not the case (Figure 4a).

The above also accounts for the difference in fitted contact angles in the parallel direction (Figure 3b). For larger volumes, the droplet spreads too far and recedes after impact, giving rise to contact angles closer to the receding values; as such, the trend decreases for larger droplets. The impact also affects the perpendicular contact angle $\theta_{\perp}$. For the largest droplet with the highest impact energy, the liquid has wetted too many stripes. The droplet attempts to retract from these stripes, but because of the hindrance of the receding motion, relatively small contact angles are observed. The diameter of the deposited droplet always ends up being larger than the equilibrium diameter on PFDTS, where the contact angle is 106°. In summary, because of the finite kinetic energy for all droplets considered until now, the width is larger than for a droplet when it would be deposited without any kinetic energy.

To minimize the kinetic impact energy of the droplet, we produced larger liquid volumes by sequentially firing multiple picoliter droplets. In that case, the liquid puddle already present on the surface acts as a "cushion", absorbing the kinetic energy and therewith lowering the kinetic effects as the liquid volume on the surface increases. The nozzle is set to fire 600 pL droplets every 0.1 s. For the first few droplets, we again observe the spherical flattened shape as described above. However, with time the droplet grows and starts to elongate. Figure 5a depicts the aspect ratio of the droplets as a function of α at different times during the sequential firing, corresponding to different volumes of 40, 160, and 1000 nL. (These volumes correspond to spherical droplets with diameters of 0.42, 0.67, and 1.24 mm.)

For the 40 nL droplet, consisting of 67 droplets of 600 pL each, the effective absorption of kinetic energy is already visible by the elongation of the droplets; the aspect ratio is similar to that of the 1 μL droplets deposited by the syringe. After prolonged firing (i.e., for a larger total volume of 160 nL), the aspect ratio becomes markedly larger than that of the 40 nL droplet for all α, even exceeding the values for the 1 μL droplets in Figure 1. When we continue to deposit, the aspect ratio is still increasing; for the 1000 nL droplet with a volume equal to that in Figure 1, the aspect ratio is considerably larger. Apparently, for these composed droplets the impact diameter is relatively small. This prevents the movement of the contact line over a hydrophobic PFDTS stripe. The added volume during firing will move in the direction parallel to the stripes, giving rise to longer droplets with larger aspect ratios. The width of the droplet deposited in this way is smaller than when a droplet is deposited with a syringe. This can also be seen in the number of stripes that is spanned by the droplet. The number of stripes spanned by the 1 μL droplet created by multiple droplets is between 100 and 250 stripes (depending on α). In comparison, for the syringe case this amounts to 150 and 375 stripes.

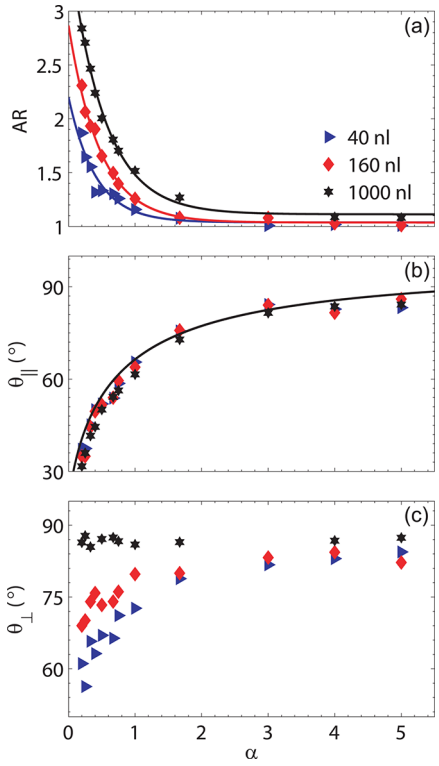

Figure 5. (a) Aspect ratio as a function of α for continuously deposited droplets. The solid lines are a guide to the eye. (b) Parallel contact angle $\theta_{\parallel}$ exhibiting identical scaling with α for all volumes; the black line corresponds to eq 1 with $\theta_{PFDTS} = 98°$ and $\theta_{SiO_2} = 20°$. (c) Perpendicular contact angle $\theta_{\perp}$ as a function of α.

In Figure 5b,c, the parallel and perpendicular contact angles are plotted as a function of α. As with the single-shot picoliter droplet, $\theta_{\parallel}$ still scales as a function of α following the Cassie–Baxter model. However, now there is no difference with varying volumes. Because the liquid puddles were created by multiple much smaller droplets, the contact angle is expected to resemble the advancing contact angle rather than the receding ones, as was the case for the single picoliter droplets. However, the contact angle is still close to the receding values, indicating that surface waves generated by the impact still push the droplet a bit further, leading to receding contact angle values.

It is more interesting to focus on the perpendicular contact angles because kinetics has a greater influence there. For the 40 nL droplet, $\theta_{\perp}$ is lowest in comparison to those for the other volumes and increases with α. For larger droplets, $\theta_{\perp}$ increases; for the 1000 nL droplet, a static contact angle is observed, with little dependence on α. The perpendicular contact angle is lower than the fit angle that is used for the Cassie–Baxter model; apparently there is still some kinetic energy introduced by the firing leading to perpendicular contact angles that are closer to the receding contact angle on PFDTS, which decreases as the wafer becomes contaminated over time.

The change in contact angle for the different volumes is due to hysteresis that is present on the surface. For the relatively low volume droplets (40 and 160 μL), the kinetic energy that is introduced by a new droplet is high enough to cross the PFDTS barriers, leading to a wider droplet. Once the droplet has passed the PFDTS stripes, it is unable to recede back over the SiO_2 stripes, leading to a lower contact angle. This is the same principle as shown in Figure 4.

Comparing the results for both deposition methods with markedly lower aspect ratios of droplets deposited by the syringe, we conclude that the latter approach still induces considerable kinetic energy into the system, ultimately leading to more wetted stripes and thus larger widths. High-speed-camera movies indeed confirm the presence of capillary waves due to detachment from the dispensing needle, introducing kinetic energy at the contact line.

The contact angles on the pristine surfaces of PFDTS and SiO_2 are comparable for water and glycerol. Both liquids also have approximately the same surface tension, so one would expect roughly the same AR as a function of α. This is not the case when comparing 1 μL water (Figure 1) and glycerol[15] droplets deposited from a syringe. Glycerol is much more viscous than water (1400 and 0.9 mPa/s, respectively) and as such gives rise to a more gentle deposition process, leading to higher aspect ratios.

In the dispersion relation of capillary waves (i.e., the complex frequency vs the wave vector), a transition is typically observed from overdamped to propagating behavior. The transition occurs at a critical wavelength that can be approximated by $\lambda_c \approx (\eta^2)/(\sigma\rho)$, where η is the dynamic viscosity, σ is the surface tension, and ρ is the liquid density.[27] Considering our system, we find values for the critical capillary wavelength of $\lambda_c \approx 14$ nm for water and $\lambda_c \approx 2.5$ cm for glycerol. This implies that a 1 μL droplet as considered here is in the overdamped regime for glycerol whereas it is in the propagating regime for water. This is also reflected by the Ohnesorge number, which can be rationalized as the ratio of the relevant length scale of our system (typically 10 μm) and the critical capillary length. The actual values of the Ohnesorge number are smaller than 1 for water and much larger than 1 for glycerol. This obviously gives rise to marked differences in dynamic spreading behavior and therewith the final aspect ratio of the droplets, as observed in our experiments. By eliminating the influence of these waves on water droplets, we see that our present 1000 nL multidrop results are very similar to those with glycerol droplets of the same volume, as presented in the past.[15]

■ CONCLUSIONS

We have performed a thorough investigation of the effect of kinetic energy during droplet impact on chemically striped patterned surfaces. Using either the deposition of microliter droplets with a conventional dosing needle or the firing of picoliter droplets by means of an inkjet printhead has enabled us to tune the effect of kinetics on the final shape of the droplets. When the kinetic effects are negligible, the droplets exhibit strong elongation due to preferential spreading along the stripes. However, for high impact energies the substantial initial isotropic spreading gives rise to much wider droplets, with aspect ratios even below unity. Our results clearly demonstrate the profound influence of kinetic energy on the directional wetting of anisotropically patterned surfaces, which is in agreement with the comparable case of droplets spreading on corrugated surfaces.

■ AUTHOR INFORMATION

Corresponding Author

*E-mail: e.s.kooij@utwente.nl. Phone: +31 (0)53 4893148. Fax: +31 (0)53 4891101.

Notes

The authors declare no competing financial interest.

■ ACKNOWLEDGMENTS

We thank M. van der Meulen (University of Twente) for assistance with equipment and J. H. Snoeijer (University of Twente) for helpful discussions. For providing access to the Kruss DSA 100M system, Joanneum Research (Styria) is acknowledged. This work is supported by NanoNextNL, a micro- and nanotechnology consortium of the Government of The Netherlands and 130 partners.

■ REFERENCES

(1) Drelich, J.; Wilbur, J. L.; Miller, J. D.; Whitesides, G. M. Contact angles for liquid drops at a model heterogeneous surface consisting of alternating and parellel hydrophobic/hydrophilic strips. *Langmuir* **1996**, *12*, 1913.
(2) Lipowsky, R. Morphological wetting transitions at chemically structured surfaces. *Curr. Opin. Colloid Interface Sci.* **2001**, *6*, 40−48.
(3) Brinkmann, M.; Lipowsky, R. Wetting morphologies on substrates with striped surface domains. *J. Appl. Phys.* **2002**, *92*, 4296−4306.
(4) Iwamatsu, M. Contact angle hysteresis of cylindrical drops on chemically heterogeneous striped surfaces. *J. Colloid Interface Sci.* **2006**, *297*, 772−777.
(5) Wang, X.-P.; Qian, T.; Sheng, P. Moving contact line on chemically patterned surfaces. *J. Fluid Mech.* **2008**, *605*, 59−78.
(6) Vellingiri, R.; Savva, N.; Kalliadasis, S. Droplet spreading on chemically heterogeneous substrates. *Phys. Rev. E* **2011**, *84*, 036305.
(7) Darhuber, A. A.; Troian, S. M.; Miller, S. M.; Wagner, S. Morphology of liquid microstructures on chemically patterned surfaces. *J. Appl. Phys.* **2000**, *87*, 7768−7775.
(8) Kusumaatmaja, H.; Yeomans, J. M. Modeling contact angle hysteresis on chemically patterned and superhydrophobic surfaces. *Langmuir* **2007**, *23*, 6019−6032.
(9) Jansen, H. P.; Bliznyuk, O.; Kooij, E. S.; Poelsema, B.; Zandvliet, H. J. W. Simulating anisotropic droplet shapes on chemically striped patterned surfaces. *Langmuir* **2012**, *28*, 499−505.
(10) David, R.; Neumann, A. W. Anisotropic drop shapes on chemically striped surfaces. *Colloids Surf., A* **2012**, *393*, 32−36.
(11) David, R.; Neumann, A. W. Shapes of drops in the Cassie state on grooved surfaces. *Colloids Surf., A* **2012**, *399*, 41−45.
(12) Gleiche, M.; Chi, L.; Gedig, E.; Fuchs, H. Anisotropic contact-angle hysteresis of chemically nanostructured surfaces. *ChemPhysChem* **2001**, *2*, 187−191.
(13) Morita, M.; Koga, T.; Otsuka, H.; Takahara, A. Macroscopic-wetting anisotropy on the line-patterned surface of fluoroalkylsilane monolayers. *Langmuir* **2005**, *21*, 911−918.
(14) Chung, J. Y.; Youngblood, J. P.; Stafford, C. M. Anisotropic wetting on tunable micro-wrinkled surfaces. *Soft Matter* **2007**, *3*, 1163−1169.
(15) Bliznyuk, O.; Vereshchagina, E.; Kooij, E. S.; Poelsema, B. Scaling of anisotropic droplet shapes on chemically stripe-patterned surfaces. *Phys. Rev. E* **2009**, *79*, 041601.
(16) Bliznyuk, O.; Jansen, H. P.; Kooij, E. S.; Poelsema, B. Initial spreading kinetics of high-viscosity droplets on anisotropic surfaces. *Langmuir* **2010**, *26*, 6328−6334.
(17) Bliznyuk, O.; Veligura, V.; Kooij, E. S.; Zandvliet, H. J. W.; Poelsema, B. Metastable droplets on shallow-grooved hydrophobic surfaces. *Phys. Rev. E* **2011**, *83*, 041607.
(18) Bliznyuk, O.; Jansen, H. P.; Kooij, E. S.; Zandvliet, H. J. W.; Poelsema, B. Smart design of stripe-patterned gradient surfaces to control droplet motion. *Langmuir* **2011**, *27*, 11238−11245.
(19) Kooij, E. S.; Jansen, H. P.; Bliznyuk, O.; Poelsema, B.; Zandvliet, H. J. W. Directional wetting on chemically patterned substrates. *Colloids Surf., A* **2012**, http://dx.doi.org/10.1016/j.colsurfa.2011.12.075.
(20) Xia, D.; Johnson, L. M.; López, G. P. Anisotropic wetting surfaces with one-dimesional and directional structures: fabrication approaches, wetting properties and potential applications. *Adv. Mater.* **2012**, *24*, 1287−1302.
(21) Kannan, R.; Sivakumar, D. Drop impact process on a hydrophobic grooved surface. *Colloids Surf., A* **2008**, *317*, 694−704.
(22) Kannan, R.; Sivakumar, D. Impact of liquid drops on a rough surface comprising microgrooves. *Exp. Fluids* **2008**, *44*, 927−938.
(23) Léopoldès, J.; Bucknall, D. G. Droplet spreading on micro-striped surfaces. *J. Phys. Chem. B* **2005**, *109*, 8973−8977.
(24) Kusumaatmaja, H.; Vrancken, R. J.; Bastiaansen, C. W. M.; Yeomans, J. M. Anisotropic drop morphologies on corrugated surfaces. *Langmuir* **2008**, *24*, 7299−7308.
(25) Cassie, A. B. D.; Baxter, S. Large contact angles of plant and animal surfaces. *Nature* **1945**, *155*, 21−22.
(26) Clanet, C.; Béguin, C.; Richard, D.; Quéré, D. Maximal deformation of an impacting drop. *J. Fluid Mech.* **2004**, *517*, 199−208.
(27) Madsen, A.; Seydel, T.; Sprung, M.; Gutt, C.; Tolan, M.; Grübel, G. Capillary waves at the transition from propagating to overdamped behavior. *Phys. Rev. Lett.* **2004**, *92*, 096104.